JSEE Vol. 26, No. 4, 2024 DOI: 10.48303/jsee.2024.2035067.1111

Research Paper

Numerical Study on Mitigating Dynamic Compaction Transient Waves Using Open Trenches and Borehole Barriers

AmirReza Kermani[1], Amir Hamidi[2], Navid Fathi Afshar[3] and Farhad Asemi[3]*

1. Graduate student, Department of Civil Engineering, School of Engineering, Kharazmi University, Tehran, Iran
2. Professor, Department of Civil Engineering, School of Engineering, Kharazmi University, Tehran, Iran,
*Corresponding Author; email: hamidi@khu.ac.ir
3. Ph.D. candidate, Department of Civil Engineering, School of Engineering, Kharazmi University, Tehran, Iran

Received: 09/07/2024
Accepted: 23/07/2024

Keywords:
Dynamic compaction; Barrier; Borehole; Open trench; PPV; Vibration

ABSTRACT

Dynamic compaction in urban areas has great potential to damage nearby structures and their occupants due to induced vibrations. One common approach to keeping these vibrations in a safe range is installing a barrier crossing the wavefronts. Previous studies have largely focused on evaluating the effectiveness of trench barriers in reducing continuous vibrations, while the efficiency of boreholes as an alternative approach with a lower volume of excavation has not been thoroughly investigated. This study uses ABAQUS software to compare the efficiency of borehole and trench barriers in reducing vibrations induced by the dynamic compaction (DC) process using a 3D model validated by in-field study results. The study uses a row of hollow boreholes with varying diameters, depths, and center-to-center distances located at a fixed location from the tamping point to investigate the efficiency of borehole barriers based on their geometrical parameters. Open trenches with varying lengths, depths, and distances from the tamping point are also used for comparative investigations. The results indicate that the trenches have overall better performance than borehole barriers. However, properly designed boreholes can still reduce vibrations to an acceptable extent. Finally, the study presents design guidelines for further practical applications.

How to cite the article:
Kermani, A. , Hamidi, A. , Fathi Afshar, N. and Asemi, F. (2024). Numerical study on mitigating dynamic compaction transient waves using open trenches and borehole barriers. *Journal of Seismology and Earthquake Engineering*, *26*(4), 37-52. doi: 10.48303/jsee.2024.2035067.1111

1. Introduction

With the increase in population and urbanization, there has been a growing interest in improving loose lands. Dynamic Compaction (DC) is one of the most effective soil improvement methods (Abedini et al., 2022). Although Dynamic Compaction improves the surrounding soils, the vibrations caused by the impact can adversely affect nearby structures. These effects include settlement and cracks in buildings, disturbance to occupants, and damage to pipelines (Majumder & Venkatraman, 2023). To prevent structural damage, the generated peak particle velocity (PPV) must be kept within an acceptable range (Mehdipour & Hamidi, 2017, Hamidi et al., 2018). To ensure this, previous studies have provided the maximum and minimum allowable PPV values for structures with different vibration level sensitivity (Hamidi et al., 2018, 2019). The vibration values exceeding the allowable range must be kept within the safe area by employing different approaches such as changing the vibration characteristics of the excitation source, improving the damping properties of the soil, or installing a barrier to intercept the wavefronts.

The methods for isolating propagating waves can be classified into two types based on the relative location of the barrier and the excitation source. These types are called active when the source is isolated or where the distance between the barrier and the vibration source is less than one times the Rayleigh wavelength (i.e. 1λ) (Klein et. al., 1997; Yang & Hung, 1997) and passive when the structure is isolated or where the distance is greater than or equal to five times the Rayleigh wavelength (5λ) (Al-Hussaini & Ahmad, 1996; El Naggar & Chehab, 2005).

Generally, barriers can be classified as stiff, soft, or hollow (or open) based on the properties of the filling materials. The overall performance of barriers depends on their ability to reflect, diffract, and scatter the wavefronts (Liu et al., 2018). Studies have shown that soft barriers filled with material softer than the surrounding soils are more effective than stiff barriers (Hung et al., 2004; El Naggar & Chehab, 2005; Adam & von Estorff, 2005). Most researchers agree that hollow trenches are more efficient than filled ones (Celebi et.al., 2009). However, due to the instability of the side walls of hollow trenches, especially at great depths, filled barriers have been regarded as a better alternative approach.

Over the years, different researchers have investigated geometrical parameters, including length, width, and height of barriers, as well as the physical properties of their filling materials numerically and experimentally. Field studies have shown that the ratio of trench height to the Rayleigh wavelength plays an important role in its performance (Woods et al., 1974; Richart et al., 1970). Numerical studies have also revealed that increasing the trench depth enhances its effectiveness (Al-Hussaini & Ahmad, 1996; El Naggar & Chehab, 2005; Tsai & Chang, 2009; Ekanayake et.al., 2014; Hamidi & Farshi Homayoun Rooz, 2021). However, other studies have shown a critical depth at which the barriers reach their maximum performance (Qiu et al., 2014; Saikia & Das, 2014; Kermani et al., 2024). The results of both in-field studies (Woods, 1968) and numerical studies (Saikia & Das, 2014; Liu et al., 2020) have indicated that the width of a barrier has little effect on its performance. However, in the case of water-filled barriers, increasing the width of the barriers can enhance the performance (Ekanayake et al., 2014).

Previous numerical studies have shown that the length parameter has subtle effect on the barrier performance (Ekanayake et al., 2014; Zoccali et al., 2015). Some studies revealed that the largest reduction in vibrations occurs up to a particular distance behind the barrier. Beyond this distance, vibrations gradually increase (Chew & Leong, 2019; Fathi Afshar et al., 2024; Kermani et al., 2024). Naghizadehrokni et al. (2020) showed that this optimal distance for geofoam barriers is around 0.7λ to 1λ.

Previous studies have mainly focused on isolating ground vibrations caused by a continuous excitation source, which includes specific amplitude and frequency and is repeated in numerous cycles, such as machine operations, train traffic loads, and vibratory pile driving. However, the effect of barriers on reducing transient vibrations, similar to those induced during the dynamic compaction process, has not been the main focus of previous research. Therefore, this study aims to evaluate the effect of borehole and trench barriers on mitigating

the induced vibrations during the DC process using numerical investigations in Abaqus-3D software. The study discusses the effects of the barriers' geometrical parameters on their performance and provides some performance tables. The presented tables can serve as an insightful guideline for further practical applications to design a barrier with a desired level of reduction in vibrations.

2. Selection of an Appropriate Parameter to Assess Transient Vibrations

Different methods have been employed to evaluate vibrations induced by human activities. These methods include Peak Particle Displacement (PPD), Peak Particle Acceleration (PPA), and Peak Particle Velocity (PPV). The PPV parameter has been widely utilized by researchers and has shown a strong correlation with the inception of structural damage (New, 1986; Kennedy, 1990; Massarsch & Broms, 1991; Abdel-Rasoul & Mohamed, 2006; Farshi Homayoun Rooz & Hamidi, 2017; Farshi Homayoun Rooz et al., 2018; Hamidi et al., 2018; Farshi Homayoun Rooz & Hamidi, 2019). Therefore, this parameter was used in this study to evaluate vibrations. It is worth noticing that depending on the wave propagation direction, particle velocity can contain three different components proportional to the spatial axes. The component in the same direction as the wave propagation is called longitudinal or radial velocity (V_R), the component perpendicular to the wave propagation direction is called vertical velocity (V_V), and the component perpendicular to both vertical and radial directions is called tangential velocity (V_T). Previous studies have utilized various methods to define the PPV value, including:

a) The Peak Vector Sum (PVS): This approach is the most accurate method for determining the PPV using the maximum value of the velocity resultant vector. According to Equation (1), the resultant vector of velocity must be calculated using the values of the three velocity components recorded simultaneously.

$$PPV = max\left(\sqrt{(V_R^2)+(V_V^2)+(V_T^2)}\right) \quad (1)$$

V_R, V_V, and V_T are the velocities in radial, vertical, and tangential directions respectively recorded simultaneously.

b) The Square Root of Squares Sum (SRSS): This method calculates the value of the resultant vector by using the maximum recorded velocity of each direction, without considering the time of occurrence. Equation (2) outlines the calculation criteria:

$$PPV = \max\left(\sqrt{(V_{R\max}^2)+(V_{V\max}^2)+(V_{T\max}^2)}\right) \quad (2)$$

where $V_{R\max}$, $V_{V\max}$, and $V_{T\max}$ represent the maximum recorded values of velocity components during the entire construction period without considering the occurrence time.

c) The Peak Unidirectional Velocity: In this approach, according to Equation (3), the peak velocity for each direction is obtained among all recorded values throughout the entire construction period. The maximum of these values is then considered as the PPV, irrespective of direction.

$$PPV = \max\left(V_{R\max}.V_{V\max}.V_{T\max}\right) \quad (3)$$

Peak Vertical Velocity (PVS): In this approach, according to Equation (4), the maximum value of the vertical component is considered the PPV. Among the various methods available, this approach has been widely used in previous research and codes, including Attewell & Farmer (1973), Massarsch & Broms (1991), Swiss Standard SN640312 (SNV, 1992), Swedish Standard SS 02 52 11 (SIS, 1999), Whenham et al. (2009), Rezaei et al. (2016), and Hamidi et al. (2018).

$$PPV = \max\left(V_{V\max}\right) \quad (4)$$

The peak vertical velocity method (d) was employed in this study for several reasons. This method is relatively simple and easy to calculate compared to others. It has been widely used in previous studies and standards, demonstrating an acceptable consistency with structural damage inception.

Moreover, it has shown a good correlation with the PVS method, which is considered the most accurate approach for calculating PPV inferred from previous investigations by Hamidi et al. (2018).

3. Numerical Modeling and Verification

The numerical simulations were performed using Abaqus-2020 finite element software, employing an implicit dynamic integration scheme. A 3D model was developed based on the soil and tamper characteristics identified in the field investigations by Fathi Afshar et al. (2024) for verification purposes. The model was then used to conduct further parametric analyses, which were the primary objective of this study.

3.1. Constitutive Model

In several numerical models of dynamic compaction, an elastic model has been assigned to soil behavior (Wang et al., 2017). However, as the soil can undergo permanent plastic deformations and yield during heavy compression, it is essential to consider its plastic behavior as well. To address this, the cap plasticity constitutive model is proved to be an effective alternative for simulating dynamic compaction (Ghanbari & Hamidi, 2014, 2015; Pourjenabi & Hamidi, 2015; Wang et al., 2017). This model considers the strain hardening and softening of the material due to multiple dynamic loading-unloading cycles. In this study, the cap plasticity model with two yield surfaces, including the fixed yield surface of the Drucker-Prager model (to represent shear failure) and movable caps to define hardening by changes in volumetric strain was used.

The fixed and moving yield surfaces of the cap plasticity model in the first and second stress invariants space ($J_1 - \sqrt{J_{2D}}$) are shown in Figure (1). These surfaces can be determined using the Equations (5) and (6):

$$f_1 = \sqrt{J_{2D}} - \alpha J_1 - \kappa = 0 \tag{5}$$

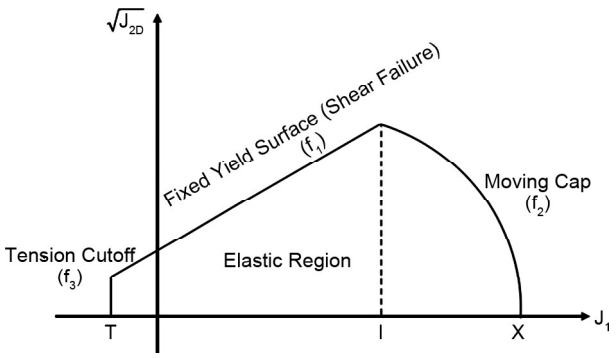

Figure 1. Yield surface of cap model in stress space.

$$f_2 = (J_1 - l)^2 + R^2 J_{2D} - (X - l)^2 = 0 \tag{6}$$

where α and k are the constants of the Drucker-Prager failure criterion, J_1 is the first invariant of the stress tensor, $\sqrt{J_{2D}}$ is the second invariant of the deviatoric stress tensor, l is the value of J_1 at the intersection point of these two surfaces, R is the ratio of the large diameter to the small diameter of the elliptic movable cap surface and X is the soil hardening parameter that depends on the plastic volumetric strain (ε_v^p).

X expresses the growth rate of the moving yield surface and can be determined according to Equation (7):

$$X = -\frac{1}{D}\ln\left(1 - \frac{\varepsilon_v^p}{W}\right) + X_0 \tag{7}$$

Here, W and D are material parameters and X_0 is the initial mean stress due to gravity analysis that represents the initial condition of the yield surface. The tension cutoff surface (f_3) limits the yield criterion based on the tensile stress state of the soil.

3.2. Verification

The study conducted by Fathi Afshar et al. (2024) investigated the effects of trench and borehole barriers on vibration isolation during a large-scale DC process. The results of the numerical modeling were validated using data extracted from this study. Following this validation, the developed numerical model was employed for further parametric investigations in the current study.

Figure (2a) shows the geometrical dimensions of the tamper used in the model. A cylindrical steel tamper filled with waste concrete, weighing 1.6 tons, with a diameter and height of 0.75 m was used. The tamper freely fell from a height of 3.6 m, transferring an approximate energy of 6 ton-m at its intersection point. The tamper was modeled separately as a rigid body under free-fall conditions on the ground surface. Each tamping stage was repeated 10 times.

The master-slave method, using the surface-to-surface technique, was utilized to simulate the soil-tamper interaction. Farshi Homayoun Rooz and Hamidi (2019) declared that this method

enhances the prediction of the soil's stresses and strains at its intersection with an external object. The penalty contact method, with a friction coefficient of 0.5, was applied to the interacting surfaces.

Figure (2b) shows the geometry of the soil medium used in this model. A cylindrical medium with a diameter of 30 meters and a height of 10 meters was used, consisting of a 2-meter clayey sand (SC) which is placed over an 8-meter low plasticity clay (CL) similar to the field studies of Fathi Afshar et al. (2024). The soil properties of these two layers are shown in Table (1). The vertical dimension of this model was chosen great enough to prevent wave reflection from the bottom boundaries. Also, the absorbent boundaries method similar to studies of Zhang and Tao, (2011) and Hamidi et al. (2018) was used to prevent wave reflection from the side boundaries. In addition, the displacements of the side boundaries were fixed in horizontal X and Y directions. They remained open in the vertical Z direction and the rotation around X, Y, and Z axes. The mesh dimensions in the area of the investigation were chosen fine enough to ensure the consistency between filed and numerical results.

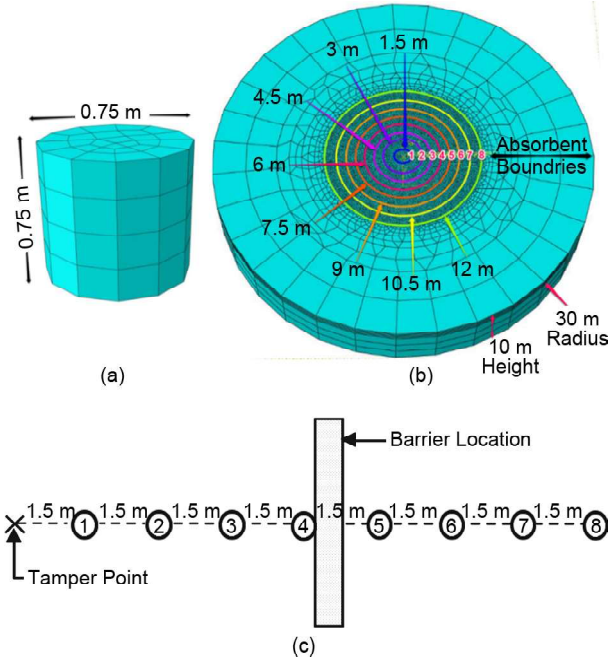

Figure 2. (a) Tamper geometry (b) Geometry of soil medium and assigned sensors (c) Location of the sensors relative to the barrier based on Fathi Afshar et al. (2024).

Figures (2b) and (2c) illustrate the locations of the sensors. According to these figures, eight sensors were installed with a center-to-center distance of 1.5 meters to record particle velocities. Similar to the field studies, these sensors were extended up to 12 meters from the tamping point along a line matching the tamping point to the barriers' center line. The distance from the first sensor to the tamping point was considered 1.5 meters, and sensor number 4 was attached exactly to the barrier sidewall on the side facing the tamping point.

Fathi Afshar et al. (2024) conducted a series of conventional triaxial shear tests to derive the cap plasticity parameters. The values of the plastic volumetric strain corresponding to each confining pressure during the first step of these tests were calculated using Equation (8), where ε_v^p represents the volumetric plastic strain, ε_v represents the total volumetric strain containing volumetric elastic and plastic strains, ε_v^e is the volumetric elastic strain, and p and K are the values of mean pressure and the bulk modulus, respectively. The plastic strains corresponding to the confining pressures from the triaxial tests are presented in Table (2).

$$\varepsilon_v^p = \varepsilon_v - \varepsilon_v^e = \varepsilon_v - \frac{p}{K} \tag{8}$$

Table 1. Upper and lower layer soil properties in numerical modeling (Data from Fathi Afshar et al., 2024).

Soil Properties										
Layer	**Classification (USCS)**	**Thickness**	γ_d	**Cohesion (C)**	**Friction Angle**	**Elastic Modulus**	**Bulk Modulus**	**Poisson's Ratio**	**Void Ratio**	**Water Content**
-	-	M	KN/m^3	Kg/cm^2	degrees	MPa	MPa	-	-	%
Upper	SC	2	14.71	0.25	31	11.77	13.04	0.35	0.8	12
Lower	CL	8	17.65	1.10	7	29.42	49.03	0.4	0.6	15

Table 2. Variation of plastic strain with confining stress in triaxial tests (Fathi Afshar et al. 2024).

Confining Stress (kPa)	49.05	98.10	147.15	196.20	245.25	294.30	343.35	392.40	441.45	490.50
ε_v^p **(%)**	0.29	0.58	0.87	1.16	1.44	1.73	2.08	2.54	3.01	3.59

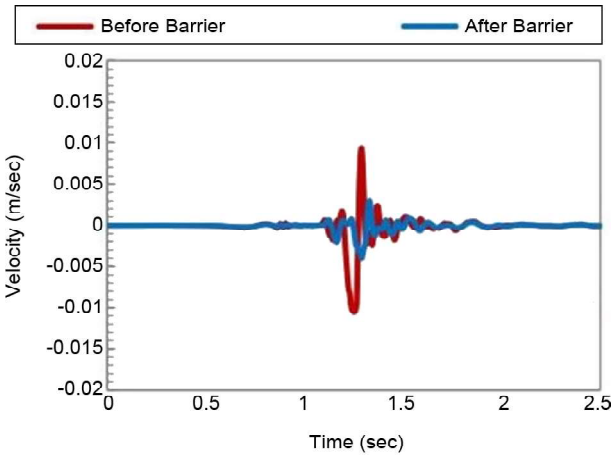

(a) Five Boreholes of 0.4 m Diameter, 0.9 m Center to Center Distance, and 2 m Depth

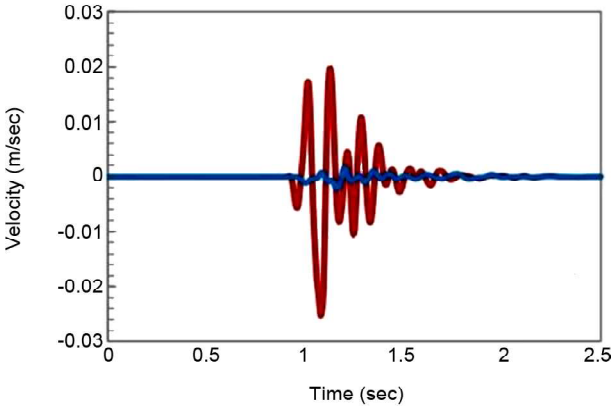

(b) A Trench of 4 m Length, 0.65 m Width, and 2.5 m Depth

Figure 3. Time history outputs for sensors number 4 and 5.

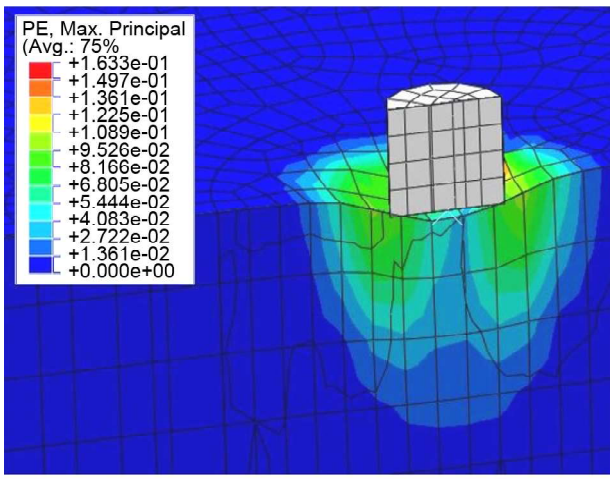

(a) The First Blow

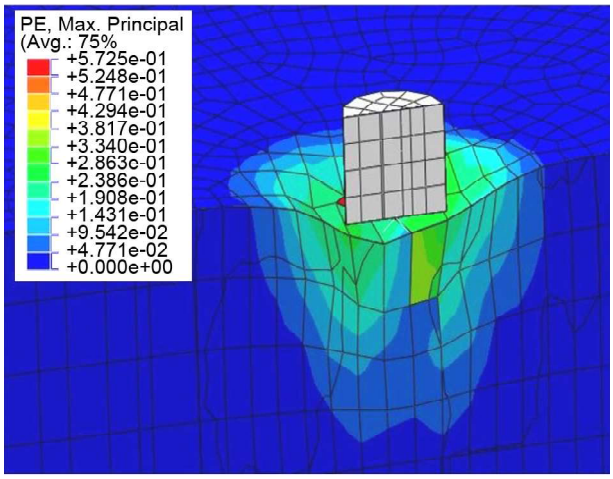

(b) The Fifth Blow

Figure 4. Plastic volumetric strain contours in numerical model of Fathi Afshar et al. (2024) field studies.

The modeling outputs were measured by vertical velocity time history diagrams for each drop, and then the pick record was extracted consequently. Figure (3) illustrates the vertical velocity time history for sensors 4 and 5, which were respectively installed before and after the barrier for one type of borehole and trench used in this study.

Figure (4) illustrates the plastic volumetric strain contours of the numerical model under the first and fifth tamping executions. As shown, the maximum rate of volumetric strains is obtained around 0.01 and 0.3 near the soil surface for these blows respectively.

The Nash-Sutcliffe efficiency method was used in this study to assess the consistency between numerical and experimental results. This method is commonly employed to calibrate, compare, and validate models, and it compares the relative magnitudes of residual variance (noise) and measured data variance (information) (Nash & Sutcliffe, 1970; Todini & Biondi, 2016). By analyzing the Nash-Sutcliffe efficiency, we can determine how well the observed and simulated data plots are matched. The NSE can be calculated using Equation (9):

$$NSE = 1 - \left[\frac{\sum_{i=1}^{n} (Y_i^{obs.} - Y_i^{sim.})}{Y_i^{obs.} - Y^{mean}} \right] \quad (9)$$

where $Y_i^{obs.}$ and $Y_i^{sim.}$ represent the ith observed and simulated values of the variable being investigated; Y^{mean} represents the mean of the observed data, and n represents the sample size. The NSE generally ranges from $-\infty$ to 1, with 1 being the ideal value. An efficiency index of 0.0 to +1.0 indicates unbiased predictions by the model, while NSE<0.0 values suggest that the observed data is a better predictor than the simulated value, indicating poor performance.

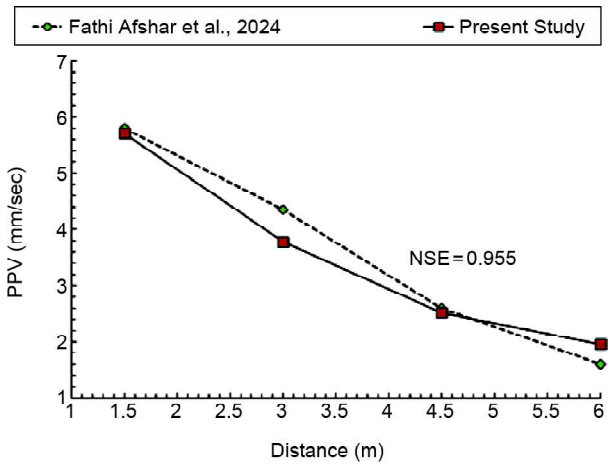

(a) 5 Boreholes of 0.4 m Diameter, 0.4 m Center to Center Distance, and 2 m Depth

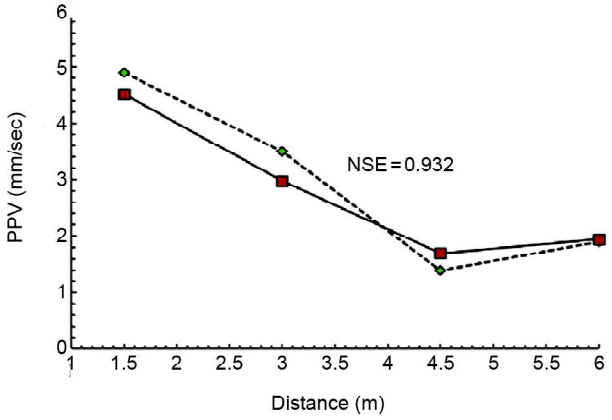

(b) A Trench of 4 m Length, 0.65 m Width, and 2 m Depth

Figure 5. Model verification for sensors number 5 to 8 in fields.

Figure (5) illustrates a comparison between the mean PPV values obtained from the numerical model and the corresponding values extracted from the field study for the sensors located behind the barrier (sensors 5 to 8) in one type of trench and borehole used in the field study. The consistency between the values obtained from the numerical and field studies shows a strong correlation between these investigations, implying the effectiveness of the model to computing vibrations.

4. Results and Discussion

4.1. Normalizing and Scaling the Values

The installation of an effective barrier with optimized dimensions and proper performance significantly depends on the soil's vibration characteristics. Therefore, it is crucial to normalize the values of the involved parameters to establish a suitable scale for future comparative studies. The Rayleigh wavelength has been widely used by previous researchers as one of the prevalent scaling factors (Woods et al., 1974; Al-Hussaini & Ahmad, 1996; Qiu et al., 2014; Ekyanke et al., 2014; Saika & Das, 2014; Ulgen & Tuygar, 2015). However, it is important to note that in such studies, the vibrations were mainly continuous and contained specific amplitudes and frequencies. Therefore, the Rayleigh wavelength could be easily calculated. In contrast, the vibrations in this study are of a transient type without specific amplitude and frequency, making the precise calculation of the Rayleigh wavelength unfeasible. Therefore, this study employs the depth of improvement recommended by the FHWA to normalize the obtained values, as defined in Equation (10),

$$d = n\left(WH\right)^{0.5} \tag{10}$$

which, d is the depth of improvement in meters, W is the mass of the tamper in Mega grams, H is the drop height in meters, and n is an empirical coefficient that is less than 1.0 and is calibrated based on the soil type. Here, the tamper weight is equal to 1.6 tons, the drop height is 3.6 m, and the n value is 0.4, therefore the d value is approximately 1 m. The dimensions of the barriers and their distances from the tamping point were normalized to this value consequently.

4.2. Parametric Study

This study employed the dimensionless velocity reduction factor (VRF) to evaluate the efficiency of boreholes and trenches. The VRF was calculated using Equation (11) for mean PPVs obtained from the 10 times repeated drops at each test. Values less than 1 show a decrease in vibration amplitude, while values greater than 1 show an increase in vibration intensity. Considering that the real effectiveness of barriers is linked to their ability to reduce the amplitude of vibrations after the barrier installation, the VRF values were measured just for sensors number 5 to 8, which were positioned beyond the barrier.

$$VRF = \frac{Peak\,Vertical\,Particle\,Velocity\,after\,Barrier\,Installation}{Peak\,Vertical\,Particle\,Velocity\,before\,Barrier\,Installation} \tag{11}$$

To better understand the calculation procedure, graphs showing the variation of PPV with respect to the distance from the tamping point have been provided in Figure (6). This figure contains the results of a field without barrier, a field with five boreholes of 0.65d diameter, 2d height and 0.9d center to center distance, and a field with a trench with length, height and thickness of 4d, 2d and 0.65d respectively. According to these graphs, it is seen that due to the effects of soil hardening at higher tamping blows, the PPV values increase with an increase in the number of blows. Additionally, for the field without barriers (Figure 6a), it is seen that the PPV values decrease almost exponentially with respect to the travelled distance from the tamping point.

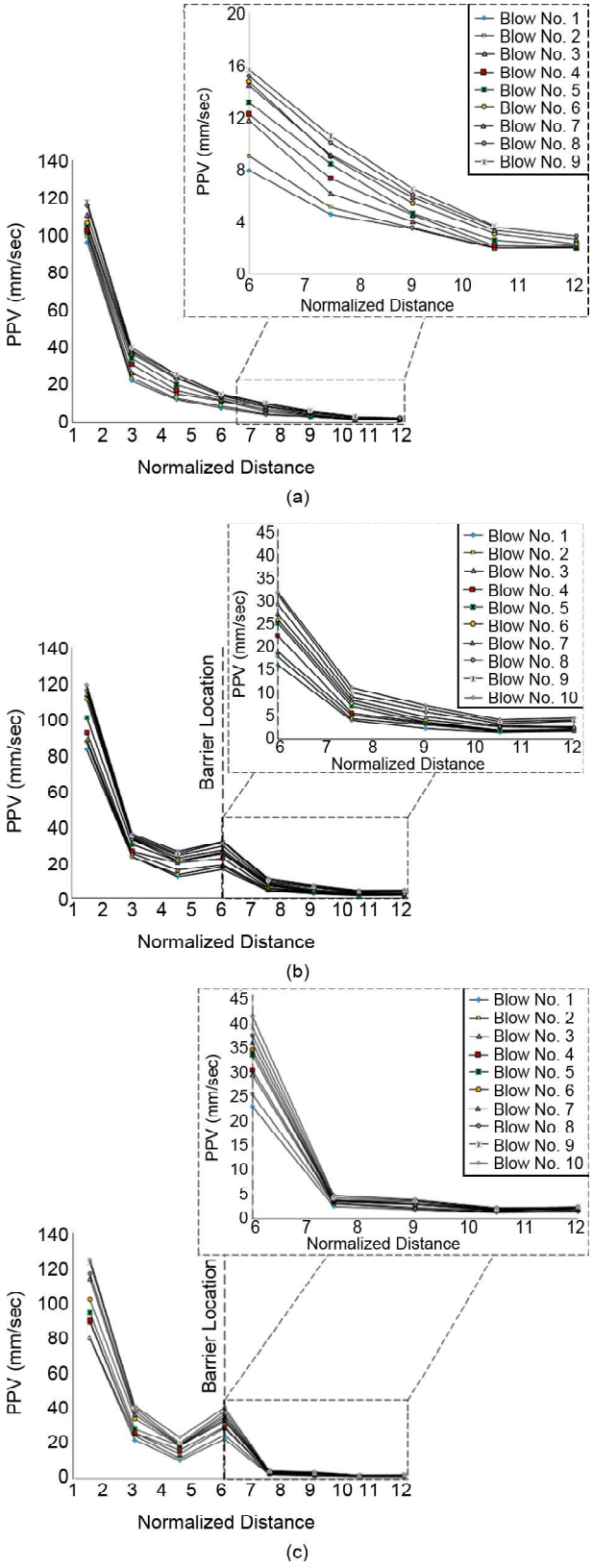

Figure 6. PPV changes with normalized distance in a ground.

According to Figure (6b), there is a slight change in the slopes of the graph for the borehole barriers, along with a minor increase in sensor number 4, which is exactly located before the barrier. This can be attributed to the interaction between the wavefront and the sidewalls of the barrier. Previous studies have revealed that this interaction leads to scattering, diffraction, and reflection of waves, causing some waves to pass through and under the barrier while others are reflected back toward the vibration source (Eslami Haghighat, 2015; Liu et al., 2018). As a result, the amplitude of vibrations increases in front of the barrier and near its anterior surface.

According to Figure (6b) and its corresponding velocity contours in Figure (7), for five boreholes with a diameter of 0.65d, a height of 2d, and a center-to-center distance of 0.9d, it is observed that while the amplitude of the vibration increases in front of the barrier in Figure (7a) (vibration-strengthened area), in Figure (7b), the amplitudes behind the barrier also increases slightly just around the last sensor (sensor number 8) located far from the barrier. According to studies by Eslami Haghighat (2015) and Liu et al. (2018), it can be concluded that due to the interaction of scattered and transmitted waves through and under the barriers and diffracted waves from the side edges, the amplitude of vibrations increases at far distances behind the barrier. This phenomenon has been shown better in Figure (7c) for a vertical section of the model. As observed, on the right side of the image where the barrier is located, the waves return to the soil surface, creating a protected area behind the barrier. In contrast, on the opposite side, the waves propagate naturally and do not tend to intersect the ground surface.

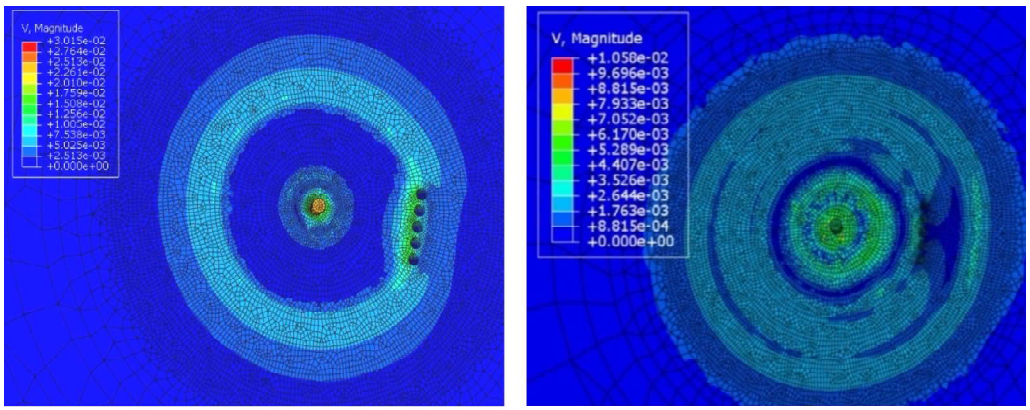

(a) 0.245 sec after Impact (b) 0.315 sec after Impact

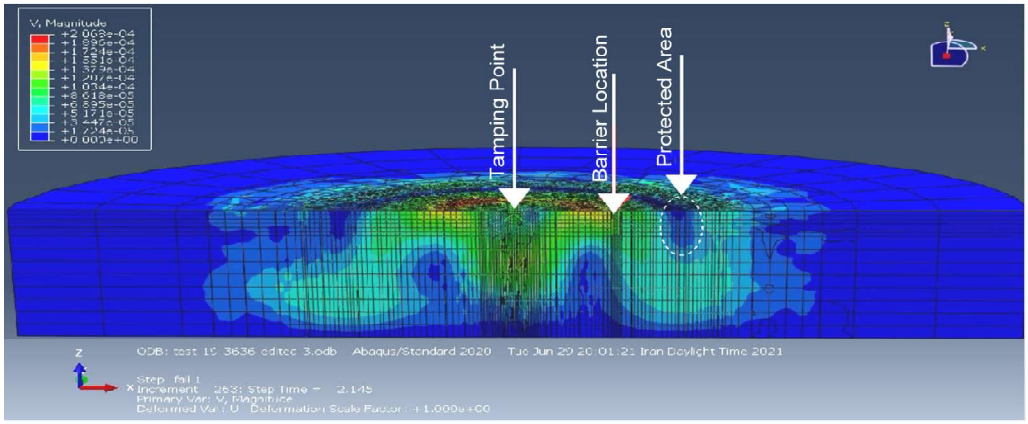

(c) A Vertical Section of This Case

Figure 7. Wave interaction with five boreholes of 0.65d diameter, 0.9d center-to-center distance, and 2d height located at 6d from the tamping point.

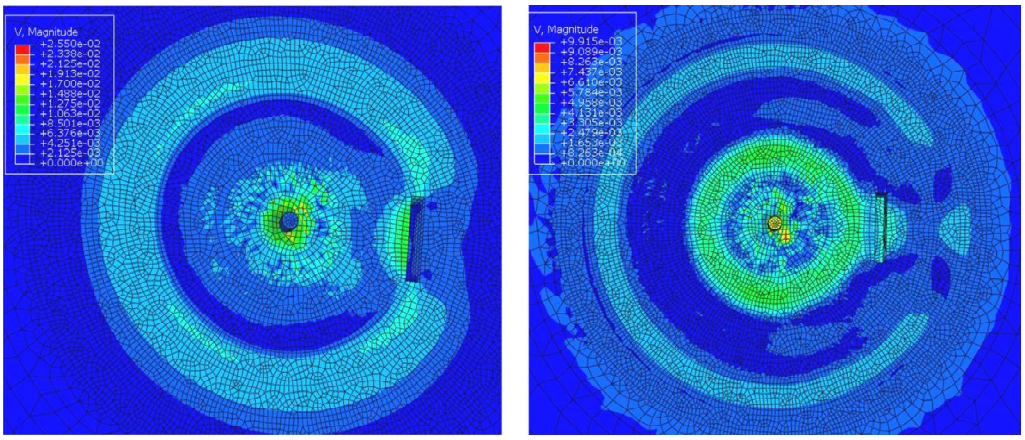

(a) 0.255 sec after Impact (b) 0.34 sec after Impact

Figure 8. Wave interaction with a trench shape barrier of 4d length, 0.65d width and 2d height located at 6d from the tamping point:

Comparing Figure (6b) with Figure (6c), a significant change in the slopes of the graphs at sensor number 4 can be observed concerning the trench barriers. This change is due to the uniform sidewalls of these barriers and the absence of any discontinuity in their geometry. As a result, it can be inferred that reducing the possibility of waves passing through the barrier leads to a greater reflection of the waves towards the vibration source with greater energy. This, in turn, results in higher amplitudes of the interacting waves in front of the barrier, as depicted in Figure (6c).

According to Figure (8), the velocity contours of this trench barrier indicate that similar to the boreholes with the same specifications, the interaction of diffracted and scattered waves from

the sides and transmitted waves under the barrier has resulted in a small increase in the vibration amplitude behind the barrier, creating a protected zone once again. These findings are consistent with the findings of previous studies conducted by Chew and Leong (2019) and Naghizadehrokni et al. (2020), which suggest the existence of a protected area behind the barrier.

4.3. Borehole Barriers

In this study, borehole barriers were examined as a potential solution for reducing the intensity of vibrations caused by dynamic compaction. Borehole barriers are considered a cost-effective option due to their smaller excavation volume compared to other types of barriers. Moreover, greater depths can be achieved by means of borehole drilling compared to trench excavation. However, the existing literature lacks extensive research on the effectiveness of such barriers. Therefore, this study aims to investigate the impact of boreholes depth, diameter, and center-to-center distance on their performance in decreasing vibrations caused by dynamic compaction. The barriers used in this study consist of five boreholes with varying geometries, located at a distance of 6d from the tamping point.

4.3.1. Effect of boreholes Distance

Figure (9) illustrates the impact of the center-to-center distance boreholes on the vibration intensity caused by dynamic compaction. Three different values of 0.4d, 0.65d, and 0.9d (where d represents the depth of improvement equal to 1 as explained earlier) were assigned to the center-to-center distance, while the diameter and depth were kept constant at 0.4d and 2d, respectively. Figure (9) indicates that decreasing the center-to-center distance increases the effectiveness of the barriers, resulting in more decay of vibrations behind the barrier. However, this positive effect is only noticeable within a protected area behind the barrier or for sensors number 5 and 6, which are located closer to the back side of the barrier. This can be deduced by the positive slope of the graphs. Additionally, for barriers with a center-to-center distance of 0.65d, while the VRF values for sensors number 5 and 6 remain below 1, and fall between the corresponding values for barriers with center-to-center distances of 0.4d and 0.9d. As the distance increases further, the VRF ratio rises and even exceeds 1. This observation indicates that for this particular barrier, the interaction of transmitted and diffracted waves amplifies the amplitude of vibrations at greater distances behind the barrier. The results demonstrate that boreholes with a center-to-center distance of 0.4d exhibit the most efficient performance due to the minimal wave transmission through the barrier. Decreasing the center-to-center distance from 0.9d to 0.4d and from 0.65d to 0.4d decreases the mean VRF of the sensors in the protected area (sensor 5 and 6) by 15% and 8%, respectively.

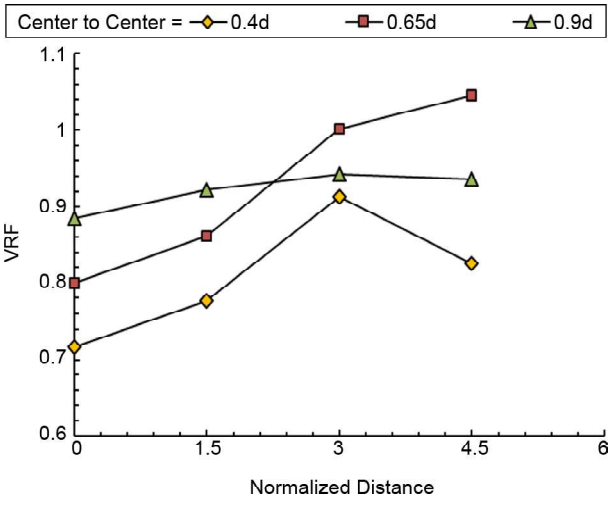

Figure 9. Effect of center-to-center distance on VRF values behind the borehole barrier:

4.3.2. Effect of Boreholes Depth

Figure (10) illustrates the effect of borehole depth on vibrations caused by DC operation. In these models, the borehole diameter and center-to-center distance were fixed at 0.4d and 0.9d, respectively. According to this figure, barriers with depths of 1.5d and 2d show the best performance. However, increasing the barrier depth beyond 2d adversely affects the performance. Additionally, the results for a barrier with a depth of 1d is obtained similar to the ground without any barrier or even slightly higher due to wave interactions. Previous studies have generally indicated that increasing the trench depth improves performance; however, there is an optimal depth relative to the Rayleigh wavelength (between 1.2 and 1.4 times) in which the performance reaches its peak (Ekanayake et

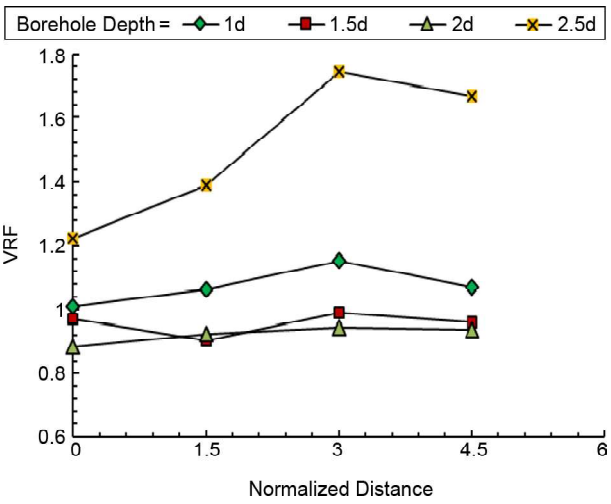

Figure 10. Effect of borehole depth on VRF values behind the borehole barrier.

al., 2014; Qiu et al., 2014; Saikia & Das, 2014). Therefore, the finding that depths greater than 2d reduce efficiency aligns well with these studies. It is worth noting that previous studies have primarily focused on investigating trench-shaped barriers, while the optimal depth of borehole barriers has not yet been comprehensively investigated.

4.3.3. Effect of Boreholes Diameter

Figure (11) illustrates the impact of borehole diameter on the reduction of vibrations caused by DC operation. The barriers in this study had fixed depths and center-to-center distances of 2d and 0.9d, respectively. This figure clearly indicates that increasing the borehole diameter from 0.4d to 0.65d, or in other words reducing the net distance between the boreholes, results in improved overall performance. This improvement is particularly tangible for sensors located closer to the back side of the barrier within the protected area. The effectiveness of the barrier gradually decreases as the distance from the barrier increases.

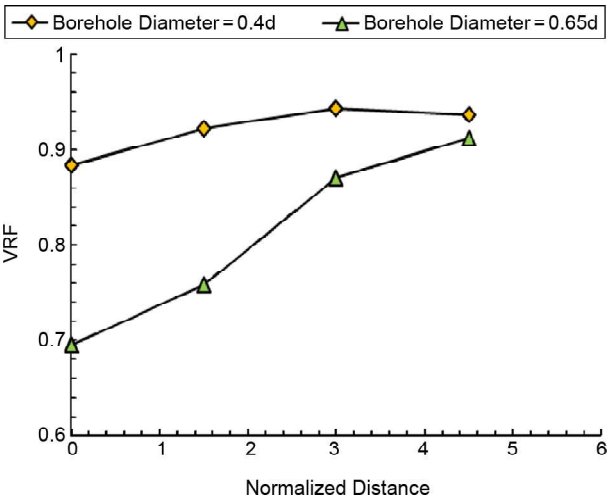

Figure 11. Effect of borehole diameter on VRF values behind the borehole barrier.

4.4. Trench Barriers

Trenches, which are rectangular-shaped barriers, are commonly used in engineering applications to mitigate ground vibrations caused by Rayleigh waves with low wavelengths. However, previous studies have not focused on the performance of these barriers in reducing transient vibrations resulting from events such as explosions in soil, impact pile driving, and dynamic compaction. Therefore, this research aims to investigate the effects of trench geometrical parameters, including depth, length, and distance from the tamping point, on reducing transient vibrations caused by DC processes

4.4.1. Effect of Trench Depth

Figure (12) depicts the impact of trench depth on VRF ratios at various distances behind the barrier. This study used four trenches, each with a fixed length of 4d, a fixed width of 0.65d, and varying depths of 1.5d, 2d, 2.5d, and 4d. All trenches were positioned 6d away from the tamping point. When comparing the results of this study to those involving borehole barriers, it is clear that trenches generally outperform boreholes in reducing vibrations. This is implicated by the lower VRF values observed behind the trenches compared to borehole barriers. Moreover, it can be inferred that while the VRFs behind the barriers at depths of 1.5d, 2d, and 2.5d exhibit a relatively similar trend, increasing the depth to 4d instantly increases the amplitude of vibrations behind the barrier. This reveals the existence of an optimal depth (less than 4d for the trenches used in this study) beyond which the performance of the barrier declines rapidly. It is worth noticing that all recorded VRF values remain less than 1, indicating the better overall performance of trenches compared to boreholes. This finding is consistent with the results of previous studies conducted by Ekanayake et al. (2014), Qiu et al. (2014), and Saikia and Das (2014).

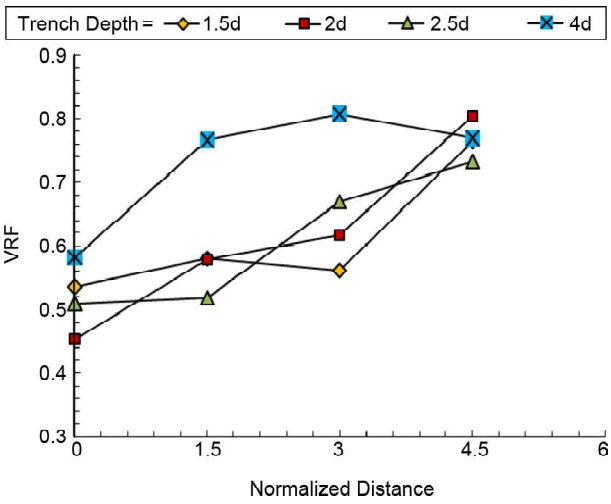

Figure 12. Effect of trench depth on VRF values behind the barrier.

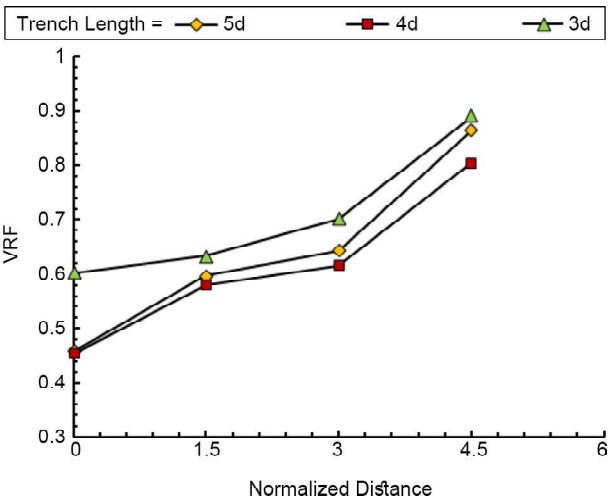

Figure 13. Effect of trench length on VRF values behind the barrier.

4.4.2. Effect of Trench Length

Figure (13) illustrates the impact of trench length on the vibrations induced by DC. The trench width, depth, and distance from the tamping point were kept constant at 0.65d, 2d, and 6d, respectively. Three different lengths - 3d, 4d, and 5d -were employed to assess the effect of trench depth. The results indicate that increasing the length from 3d to 4d slightly enhances trench performance. However, increasing the length from 4d to 5d has a negligible effect on performance.

4.4.3. Effect of Trench Location

Figure (14) illustrates the effect of trench location from the tamping point on its performance. In this section, the length, width, and depth of the trenches were fixed at 4d, 0.65d, and 2.5d, respectively. Three different installation distances of 3d, 6d, and 9d were used as the location dis-tances. The figure shows that as the distance from the tamping point increases, the trench's ability to reduce vibrations decreases. This conclusion is supported by the higher VRF values obtained behind the barrier for the trenches at farther distances compared to the trenches located closer to the tamping point. Based on these findings, it can be inferred that active isolation by trenches situated nearer to the tamping point results in better performance in vibration reduction.

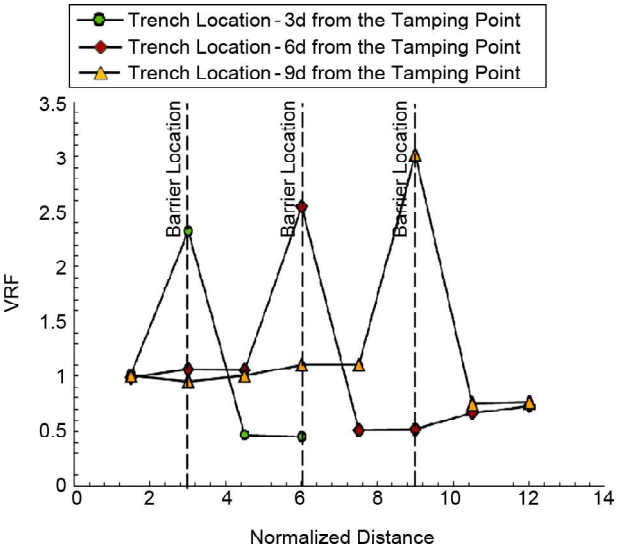

Figure 14. Effect of trench location on VRF values behind the trench barrier.

4.5. Performance Tables

In this section, the average VRF values of the sensors located behind the barrier (sensors number 5 to 8) are presented. These values serve as indicators of the barriers' overall performance. Tables (3) and (4) present the average VRF values for borehole and trench barriers used in numerical analyses. These tables provide an insightful view for further predictions of the proper geomatical parameters for a barrier with a desired level of VRF ratio. The results show that trench barriers are more effective than boreholes in reducing vibrations. The average VRF value for all trenches used in this study is approximately 0.64, indicating a 36% reduction in total induced vibrations. In contrast, the average VRF value for all borehole barriers in this study is around 0.98, highlighting their relatively poor performance. Even in some cases the average

Table 3. Comparison of borehole barriers performance.

Borehole Barriers	Distance from the Tamping Point	Diameter	Depth	Center-to-Center Distance	Average VRF Value
Fixed diameter and center-to-center distance with varying depths	6d	0.4d	1d	0.9d	1.07
			1.5d	0.9d	0.96
			2d	0.9d	0.92
			2.5d	0.9d	1.51
Fixed diameter and depth with varying center-to-center distance			2d	0.4d	0.81
			2d	0.65d	0.92
			2d	0.9d	0.92
Fixed depth and center-to-center distance with varying diameters			2d	0.9d	0.92
		0.65d	2d	0.9d	0.81
Average for all Barriers					0.98

Table 4. Comparison of trench barriers performance.

Trench Barriers	Distance from the Tamping Point	Width	Length	Depth	Average VRF Value
Fixed width and length distance with varying depths	6d	0.65d	4d	1.5d	0.611
			4d	2d	0.613
			4d	2.5d	0.607
			4d	4d	0.730
Fixed width and depth with varying lengths			3d	2d	0.710
			4d	2d	0.613
			5d	2d	0.640
Fixed width, length, and depth with varying distances from tamping point	3d		4d	2.5d	0.460
	6d		4d	2.5d	0.607
	9d		4d	2.5d	0.760
Average for all Barriers					0.64

VRF value for borehole barriers exceeds 1, indicating an increase in vibration intensity compared to the ground without any barrier. This phenomenon can be attributed to the interaction of scattered waves through the barrier and transmitted and diffracted waves from under and sidewalls of the barrier in farther distances behind it. However, the results confirm that borehole barriers are capable of reducing the post-barrier vibrations to an acceptable extent with lower excavation costs if properly designed. For instance, borehole barriers with a diameter of 0.65 d, a depth of 2 d, and a center-to-center distance of 0.9 d can reduce vibrations by 19%. Moreover, the location of the barrier plays an important role in its performance. The average VRF values for sensors positioned behind the barrier indicate that reducing the distance between the barrier and the tamping point enhances the barrier's effectiveness; trenches located at a distance of 3d from the tamping point reduced vibrations by 54%.

5. Conclusion

While dynamic compaction is considered one of the most efficient soil improvement methods, conducting this operation in vicinity of adjacent structures might cause mild to severe damage to both the structures and their occupants due to the intensity of the induced vibrations. This study aimed to examine the effectiveness of open trench and borehole barriers in screening transient vibrations caused by the DC process as a potential solution for reducing these vibrations. A series of numerical analyses was performed using Abaqus-3D software and the effects of barriers' geometrical parameters were evaluated. The key findings are outlined below:

- Generally, increasing the depth of the boreholes enhances their effectiveness. However, this study identifies an optimal depth range between 2d and 2.5d for the boreholes used in this study, beyond which the performance significantly decreases.

- Decreasing the distance between boreholes enhances their performance within the protected area behind the barrier. In farther distances from the barrier, the interaction between the diffracted waves from the sidewalls and scattered and transmitted waves through and under the barrier causes the intensity of vibrations increases slightly and the performance reduces gradually.
- Increasing the radius of the boreholes or decreasing the net distance between the sidewalls will improve the performance, specially within the protected area behind the barrier.
- For the trenches used in this study, while the performance is remained rather similar up to the depth of 2.5d, a further increase in depth results in a lower performance which emphasizes the presence of an optimum depth between these two depths.
- The effect of barrier location on its performance was investigated. The results show that by decreasing the distance from 9d to 3d, overall performance increases by 30%, indicating that active isolation for the trenches used in this study is a more effective isolation method.
- The average VRF values for the sensors behind the barrier were employed as a factor implying the overall performance of the barrier. The results show that the mean average VRF value is 0.64, indicating 36% reduction in induced vibrations. In contrast, in the case of borehole barriers, the same value is obtained 0.98 referring to the lower performance of these barriers. However, borehole barriers are capable to reduce vibrations if designed properly, with some barriers demonstrating a 19% reduction in total vibrations.

References

Abdel-Rasoul, E.I., & Mohamed, M.T. (2006). Measurement and evaluation of blasting ground vibrations and airblasts at the limestone quarries of Assiut Cement Company (CEMEX). *Journal of Engineering Sciences*, *34*(4), 1293-1309.

Abedini, F., Rafiee-Dehkharghani, R., & Laknejadi, K. (2022). Mitigation of vibrations caused by dynamic compaction considering soil nonlinearity. *International Journal of Civil Engineering*, **20**(7), 809-826.

Adam, M., & von Estorff, O. (2005). Reduction of train-induced building vibrations by using open and filled trenches. *Computers & Structures*, *83*(1), 11-24.

Al-Hussaini, T.M., & Ahmad, S. (1996). Active isolation of machine foundation by in-filled trench barriers. *Journal of Geotechnical Engineering*, *122* (4), 288-294.

Attewell, P.B., & Farmer, I.W. (1973). Modern piling: part two-attenuation of ground vibrations from pile driving. *Ground Engineering*.

Celebi, E., Firat, S., Beyhan, G., Cankaya, I., Vural, I., & Kirtel, O. (2009). Field experiments on wave propagation and vibration isolation by using wave barriers. *Soil Dynamics and Earthquake Engineering*, *29*, 824-833.

Chew, J.H., & Leong, E.C. (2019). Field and numerical modelling of sand-rubber mixtures vibration barrier. *Soil Dynamics and Earthquake Engineering*, *125*, 105740.

Ekanayake, S.D., Liyanapathirana, D.S., & Leo, C.J. (2014). Attenuation of ground vibrations using in-filled wave barriers. *Soil Dynamics and Earthquake Engineering*, *67*, 290-300.

El Naggar, M.H., & Chehab, A.G. (2005). Vibration Barriers for Shock-producing Equipment. *Canadian Geotechnical Journal*, *42*(1), 297-306.

Eslami Haghighat, A. (2015). Diffraction of rayleigh wave by simple surface irregularity using boundary element method. *Journal of Geophysics and Engineering*, *12*, 365-375.

Farshi Homayoun Rooz, A., & Hamidi, A. (2017). Numerical analysis of factors affecting ground vibrations due to continuous impact pile driving. *International Journal of Geomechanics (ASCE)*, *17*(12), Article 04017107.

Farshi Homayoun Rooz, A., Pourjenabi, M., & Hamidi, A. (2018). Allowable distance from impact pile driving to prevent structural damage considering limits in different standards. *Practice Periodical on Structural Design and Construction*, *23*(1), 04017029.

Farshi Homayoun Rooz, A., & Hamidi, A. (2019). A Numerical model for continuous impact pile driving using ALE adaptive mesh method. *Soil Dynamics and Earthquake Engineering*, *118*, 134-143.

Fathi Afshar, N., Hamidi, A., & Tavakoli Mehrjardi, G. (2024). Impact of diffraction on screening of dynamic compaction waves with barriers. *Innovative Infrastructure Solutions*, *9*, Article 184.

Ghanbari, E., & Hamidi, A. (2014). Numerical modeling of rapid impact compaction in loose sands. *Geomechanics and Engineering*, *6*(5), 487-502.

Ghanbari, E., & Hamidi, A. (2015). Improvement parameters in dynamic compaction adjacent to the slopes. *Journal of Rock Mechanics and Geotechnical Engineering*, *7*(2), 233-236.

Hamidi, A., Farshi Homayoun Rooz, A., & Pourjenabi, M. (2018). Allowable distance from impact pile driving to prevent structural damage considering limits in different standards. *Practice Periodical on Structural Design and Construction (ASCE)*, *23*(1), Article 04017029.

Hamidi, A., Farshi Homayoun Rooz, A., & Pourjenabi, M. (2019). Closure to Allowable distance from impact pile driving to prevent structural damage considering limits in different standards. *Practice Periodical on Structural Design and Construction (ASCE)*, *24*(1), Article 07018002.

Hamidi, A., & Farshi Homayoun Rooz, A. (2021). Efficiency analysis of open trench for impact pile driving through a single-variable method. *Marine Georesources & Geotechnology*, *39*(1), 82-102.

Liu, J., Feng, G., Zhang, J., Zhao, X., Yu, C., & Zhao, M. (2018). Vibration isolation mechanism of concrete piles for rayleigh waves on sand foundations. *Shock and Vibration*, 1-13.

Hung, H.H., Yang, Y.B., & Chang, D.W. (2004). Wave barriers for reduction of train-induced vibrations in soils. *Journal of Geotechnical and Geoenvironmental Engineering*, *130*(12), 1283-1291.

Hwang, J.H., & Tu, T.Y. (2006). Ground vibration due to dynamic compaction. *Soil Dynamics and Earthquake Engineering*, *26*(5), 337-346.

Kennedy, B.A. (1990). *Surface Mining* (2nd ed.). Society for Mining, Metallurgy, and Exploration.

Kermani, A., Hamidi, A., & Asemi, F. (2024). *Mitigation of Transient Vibrations Induced by Dynamic Compaction: A Numerical Study on the Efficacy of Open Trench and Borehole Barriers*. Ninth International Conference on Seismology and Earthquake Engineering, Tehran, Iran (Islamic Republic of). https://seeconferences.ir/

Klein, R., Antes, H., & Le Houédéc, D. (1997). Efficient 3D modelling of vibration isolation by open trenches. *Computers and Structures*, *64*(1-4), 809-817.

Liu, J., Yu, C., Li, K., & Wen, M. (2020). Test on the influence of geometric parameters of an annular trench on the cibration isolation area. *Shock and Vibration*, 1-19.

Majumder, M., & Venkatraman, S. (2023). A state-of-the-art review paper on the vibration screening techniques using open and in-filled trenches. *Asian Journal of Civil Engineering*, 1-16.

Massarsch, K.R., & Broms, B.B. (1991). Damage criteria for small amplitude ground vibrations. *In Proceedings of 2nd International Conference on Recent Advances in Geotechnical and Earthquake Engineering and Soil Dynamics*, Missouri Univ. of Science and Technology, St. Louis, 2, 1451-1459.

Mehdipour, S., & Hamidi, A. (2017). Impact of tamper shape on the efficiency and vibrations induced during dynamic compaction of dry sands by 3D finite element modelling. *Civil Engineering Infrastructures Journal*, *50*(1), 151-163.

Naghizadehrokni, M., Zeigler, M., & Sprenger, J. (2020). A full experimental and numerical modelling of the practicability of thin foam barrier as vibration reduction measure. *Soil Dynamics and Earthquake Engineering*, *139*, 106416.

Nash, J.E., & Sutcliffe, J.V. (1970). River flow forecasting through conceptual models part I-A discussion of principles. *Journal of Hydrology*, *10*(3), 282-290.

New, B.M. (1986). Ground vibrations caused by civil engineering works. Research Rep. No. 53,

Transport and Research Road Laboratory, Crowthorne, U.K.

Pourjenabi, M., & Hamidi, A. (2015). Numerical modeling of dynamic compaction process in dry sands considering critical distance from adjacent structures. *Structural Engineering and Mechanics*, *56*(1), 49-56.

Qiu, B., Limam, A., & Djeran-Maigre, I. (2014). Numerical study of wave barrier and its optimization design. *Finite Elements in Analysis and Design*, *84*, 1-13.

Rezaei, M., Hamidi, A., & Farshi Homayoun Rooz, A. (2016). Investigation of peak particle velocity variations during impact pile driving process. *Civil Engineering Infrastructures Journal*, *49*(1), 59-69.

Richart, F.E., Hall, J.R., & Woods, R.D. (1970). *Vibration of soils and foundations. International Series in Theoretical and Applied Mechanics*. Prentice-Hall.

Saikia, A., & Das, U.K. (2014). Analysis and design of open trench barriers in screening steady-state surface vibrations. *Earthquake Engineering and Engineering Vibration*, *13*, 545-554.

Swedish Institute for Standards (SIS). (1999). *Vibration and Shock - Guidance Levels and Measuring of Vibrations in Buildings Originating from Piling, Sheet Piling, Excavating and Packing to Estimate Permitted Vibration Levels (in Swedish), SS 02 52 11*. Stockholm, Sweden.

Swiss Association for Standardization (SNV). (1992). *Effects of Vibration on Construction, SN640312*. Winterthur, Switzerland.

Todini, E., & Biondi, D. (2016). *Calibration, Parameter Estimation, Uncertainty, Data Assimilation, Sensitivity Analysis, and Validation*. In Handbook of Applied Hydrology (2nd ed.). McGraw Hill Education.

Tsai, P.H., & Chang, T.S. (2009). Effects of open trench siding on vibration-screening effectiveness using the two-dimensional boundary element method. *Soil Dynamics and Earthquake Engineering*, *29*, 865-873.

Ulgen, D., & Toygar, O. (2015). Screening effectiveness of open and in-filled wave barriers: A full-scale experimental study. *Construction and Building Materials*, *86*, 12-20.

Wang, W., Chen, J.J., & Wang, J.H. (2017). Estimation method for ground deformation of granular soils caused by dynamic compaction. *Soil Dynamics and Earthquake Engineering*, *92*, 266-278.

Whenham, V., Areias, L., Rocher-Lacoste, F., Vié, D., Bourdouxhe, M. P., & Holeyman, A. (2009). Full scale sheet pile vibro-driving tests. *In Proceedings of the 17th International Conference on Soil Mechanics and Geotechnical Engineering*, *1, 2, 3 and 4*, 1354-1357. IOS Press.

Woods, R. D. (1968). Screening of surface waves in soil. *Journal of the Soil Mechanics and Foundations Division*, *94*(SM4), 951-979.

Woods, R.D., Barnett, N.E., & Sagesser, R. (1974). Holography: A new tool for soil dynamics. *Journal of the Geotechnical Engineering Division*, *100*(11), 1231-1247.

Yang, Y., & Hung, H. (1997). Parametric study of wave barriers for reduction of train-induced vibrations. *International Journal for Numerical Methods in Engineering*, *40*(20), 3729-3747.

Zhang, M., & Tao, M.A. (2011). Parametric study on factors affecting ground vibrations during pile driving through finite element simulations. *Geo-Risk*, 931-938.

Zoccali, P., Cantisani, G., & Loprencipe, G. (2015). Ground-vibrations induced by trains: Filled trenches mitigation capacity and length influence. *Construction and Building Materials*, *74*, 1-8.